View metadata, citation and similar papers at core.ac.uk
brought to you by CORE
provided by DSpace at VSB Technical University of Ostrava

Vol. 50 (2019) *Acta Physica Polonica B* No 3

EVOLUTION OF NUCLEAR SHAPES AND STRUCTURE IN TELLURIUM, XENON, BARIUM AND CERIUM ISOTOPES* **

M. Abolghasem, P. Alexa

Department of Physics, VŠB — Technical University of Ostrava
Ostrava, Czech Republic

A. Repko

Institute of Physics, Slovak Academy of Sciences, Bratislava, Slovak Republic

P.-G. Reinhard

University of Erlangen, Erlangen, Germany

(Received November 16, 2018)

Different Skyrme functional parametrizations were tested for Te, Xe, Ba and Ce isotopes for $N > 82$. For the SVsym34 parametrization, which best fits the experimental binding energy, potential energy curves obtained from constrained β_2, β_3 and β_4 Hartree–Fock+BCS calculations were investigated. Positions of the lowest quadrupole and octupole vibrational states and the lowest 2^+ rotational states in deformed nuclei were obtained within the Skyrme QRPA and compared to existing experimental data.

DOI:10.5506/APhysPolB.50.555

1. Introduction

The mass region above the doubly closed ^{132}Sn towards the neutron drip-line represents a challenging subject for the both experimental and theoretical nuclear structure research. New experimental radioactive beam facilities at ORNL, RIKEN or GANIL together with highly efficient arrays of HPGe detectors at neutron beam facilities (EXILL campaign at ILL) made

* Presented at the Zakopane Conference on Nuclear Physics "Extremes of the Nuclear Landscape", Zakopane, Poland, August 26–September 2, 2018.

** Supported by the SP 2018/84 project and by the National Programme for Sustainability I (2013–2020) financed by the state budget of the Czech Republic, identification code LO1406.

this region accessible for spectroscopic studies [1–3]. Chains of Te, Xe, Ba and Ce isotopes beyond $N = 82$ are of particular interest because they provide a natural laboratory to study shape and structural changes with gradually increasing number of nucleons outside doubly closed shells. From the theoretical point of view, the evolution of nuclear shapes and structural changes can be studied within algebraic models (IBM, algebraic collective model [4]) or in a more fundamental microscopic approach (mean field [5] or shell model [6]).

2. Microscopic approach with the Skyrme functional

Among self-consistent mean-field methods, the Skyrme–Hartree–Fock model is the most widely used for investigations of nuclear ground state (g.s.) deformations. The Skyrme energy density functional (SDF) $\mathcal{H}_{\rm Sk}[J_d(\vec{r})]$ depends on a set of densities $J_d(\vec{r})$. The Hamiltonian $\hat{H}$ can be heuristically obtained by variation with up to second-order functional derivatives ($\delta\mathcal{H}_{\rm Sk}[J_d(\vec{r})] = \mathcal{H}_{\rm Sk}[J_d(\vec{r}) + \delta J_d(\vec{r})] - E_0$), the first order constitutes the Hartree–Fock (HF) Hamiltonian and both the first and the second orders contribute to the Random-Phase-Approximation (RPA) Hamiltonian [7]

$$\begin{aligned}\hat{H} \;&=\; \sum_i \varepsilon_i \hat{\alpha}_i^\dagger \hat{\alpha}_i + \hat{V}_{\rm res} = \sum_d \int \frac{\delta\mathcal{H}_{\rm Sk}}{\delta J_d(\vec{r})} \hat{J}_d(\vec{r})\,{\rm d}\vec{r} \\ &+\frac{1}{2}\sum_{d,d'} \int\int \frac{\delta^2\mathcal{H}_{\rm Sk}}{\delta J_d(\vec{r})\delta J_{d'}(\vec{r}\,')} :\hat{J}_d(\vec{r})\hat{J}_{d'}(\vec{r}\,'):\,{\rm d}\vec{r}\,{\rm d}\vec{r}\,',\end{aligned} \tag{1}$$

where the single-quasiparticle energies ε_i are from HF+BCS, while the residual interaction $\hat{V}_{\rm res}$ (two-body operator) will contribute in RPA. Regular RPA solutions give energies and structure of lowest vibrational states, but not all obtained RPA solutions are physical. There is a set of zero-energy spurious solutions originating in broken symmetries of the Hamiltonian. The collective harmonic-oscillator-like Hamiltonian can be written in tensor-operator formalism as

$$\hat{H} = \frac{\hat{P}\cdot\hat{P}^\dagger}{2M} + \frac{1}{2}M\omega^2\hat{X}^2 = \frac{\hat{P}\cdot\hat{P}^\dagger}{2M} + \frac{\hbar^2\omega^2\hat{Q}^2}{2M}\,, \tag{2}$$

$[\hat{H},\hat{P}] = i\hbar^2\omega^2\hat{Q}$, $[\hat{H},\hat{Q}] = -i\hat{P}$, $[\hat{P}^\dagger,\hat{Q}] = -iM$. Zero-energy RPA solutions correspond to $\omega = 0$. Therefore $[\hat{H},\hat{P}] = 0$ and

$$\begin{pmatrix}\boldsymbol{A} & \boldsymbol{B}\\ \boldsymbol{B} & \boldsymbol{A}\end{pmatrix}\begin{pmatrix}P\\ P\end{pmatrix} = 0\,, \qquad \begin{pmatrix}\boldsymbol{A} & \boldsymbol{B}\\ \boldsymbol{B} & \boldsymbol{A}\end{pmatrix}\begin{pmatrix}Q\\ -Q\end{pmatrix} = -i\begin{pmatrix}P\\ -P\end{pmatrix}\,, \tag{3}$$

$$Q_{ij} = -i\big[(\boldsymbol{A}-\boldsymbol{B})^{-1}P\big]_{ij}\,, \tag{4}$$

where the RPA matrices $\boldsymbol{A}$, $\boldsymbol{B}$ are symmetric $n \times n$ matrices containing second functional derivatives of $\mathcal{H}_{\rm Sk}$, and ε_i at the diagonal of $\boldsymbol{A}$. If we now set $\hat{P} = \hat{J}_+/\sqrt{2}$ and $M = \Im$, the Hamiltonian in Eq. (2) transforms into the rotational Hamiltonian (in 3D space) and $\Im$ is the moment of inertia that can be calculated from

$$\Im = i \left\langle \left[\hat{P}^\dagger, \hat{Q} \right] \right\rangle = 2i \sum_{i>j} P^*_{ij} Q_{ij} \,, \tag{5}$$

and the energy of the 2^+ excited state of the g.s. rotational band $E_{2^+} = 3/\Im$ can be thus obtained from the 1^+ zero-energy spurious state (*cf.* [8]).

3. Results and conclusions

There are plenty of SDF parametrizations available in the literature. We refer here to a recent family of parametrizations derived from least-square fitting of its free parameters to a large pool of selected g.s. observables and, optionally, other nuclear properties over the whole nuclear chart (from carbon to lead) [11]. This family includes in additions three older choices, namely Sk-M*, SLy6, and SkI3, and comprise in total 18 different parametrizations. We observe that namely SV-sym34 with symmetry energy $J = 34$ MeV reproduces rather well the binding energies of Te, Xe, Ba and Ce chains [12]. In calculations using the axial SHF code SKYAX with a density-dependent δ-force interaction in the pairing channel [13], s.p. levels including ~ 10 oscillator shells were taken into account. In test calculations using Sky3D code [14], triaxiality was observed only for $N < 82$ that justifies our approach.

All studied nuclei are characterized by prolate g.s. quadrupole deformation β_2 for $86 \leq N \leq 120$ with the exception of $A > 156$ Te isotopes (see Fig. 1). Highest octupole deformations ($\beta_3 > 0.08$) are predicted for ^{144}Ba, ^{150}Ba, ^{148}Ce, and ^{150}Ce for prolate shapes only (see Fig. 2). The potential energy curves (PEC) are rather flat in β_3 thus resembling a phase-transition critical point and not a well-established octupole deformation. Hexadecapole deformation β_4 is predicted to be positive with a peak at $\beta_4 \approx 0.17$ for ^{152}Ce.

RPA calculations were performed in two model spaces: *(i)* a small model space (~ 10 oscillator shells), and *(ii)* a large model space (~ 22 oscillator shells). Positions of the lowest 2^+ quadrupole vibrational states (Fig. 3), lowest octupole vibrational states (Fig. 4) and lowest excited 2^+ states in g.s. rotational band of well-deformed nuclei (Fig. 5) were calculated.

As expected for 2^+ vibrational states, RPA works better in the spherical case and for well-deformed nuclei. It fails in transition region where the two PEC minima in β_2 (oblate and prolate) are not well-separated in energy. In this region, large amplitude calculations are necessary. In almost all cases, $K = 0^-$ octupole phonons are predicted to be the lowest ones.

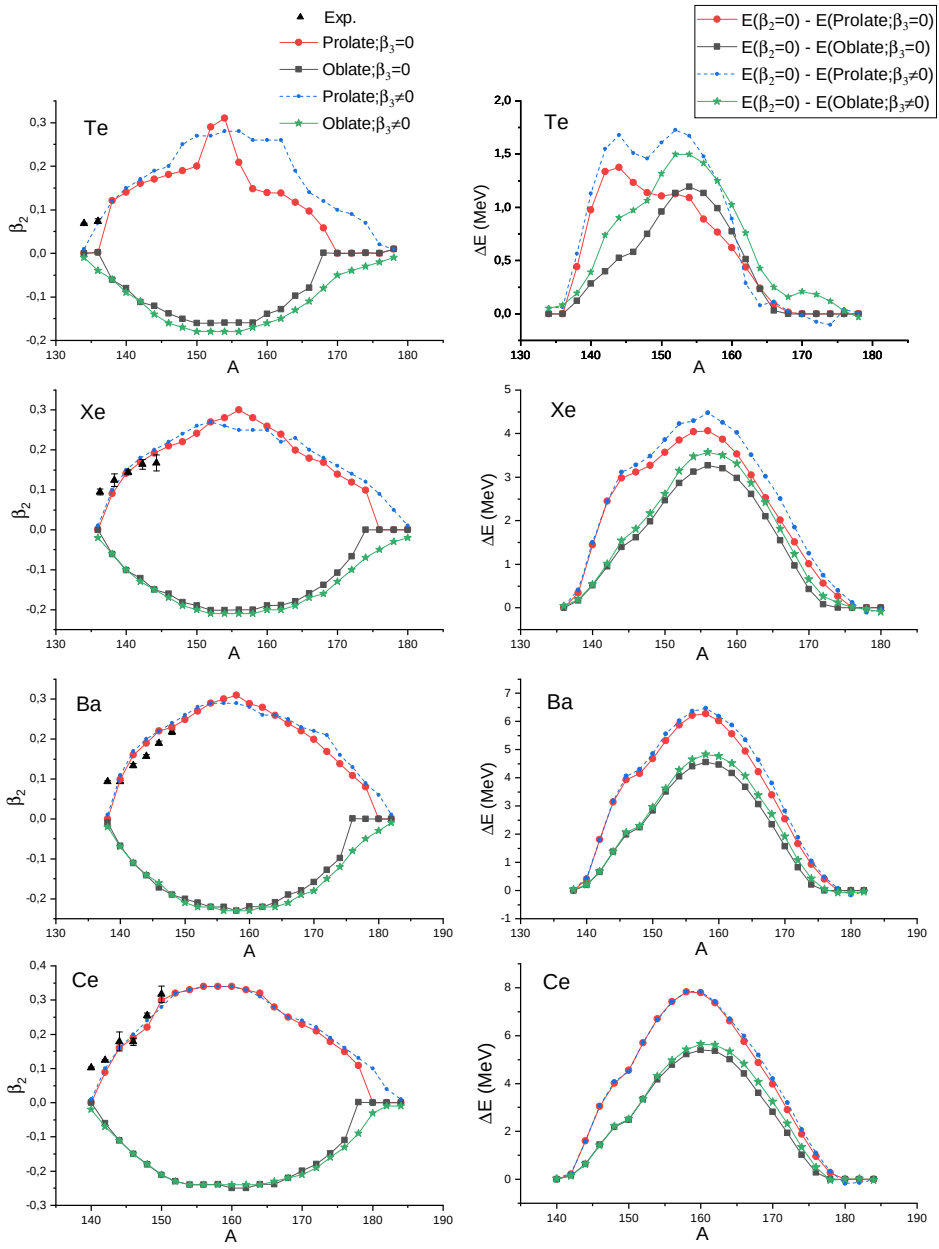

Fig. 1. Comparison of calculated and experimental [9] β_2 values and the g.s. energy excesses relative to the spherical shape with and without octupole deformation taken into account for the studied chains.

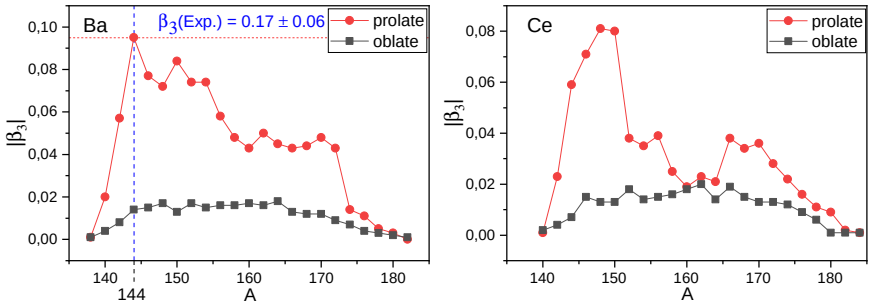

Fig. 2. Evolution of octupole deformation β_3 in Ba and Ce chains. The experimental value is taken from [10].

Again, the results obtained with the larger model space are closer to the experimental data. Positions of 2^+ g.s. band rotational states are reasonably well-reproduced for deformed nuclei. Here, the size of the model space is not critical, but the larger model space gives slightly better results.

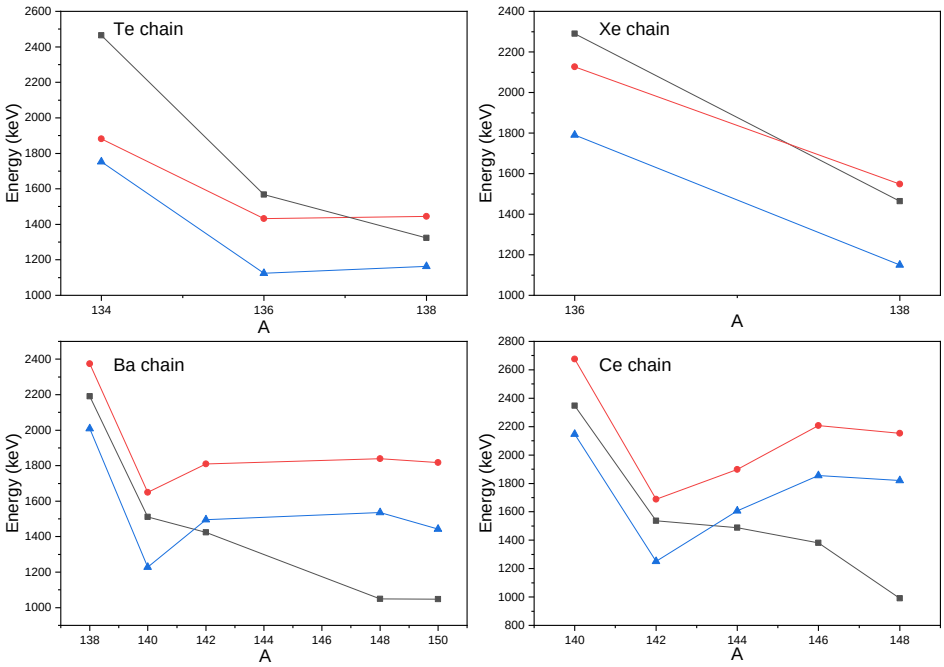

Fig. 3. Comparison of calculated (circle — small basis, triangle — large basis) and experimental (square) [15] energies of the lowest 2^+ vibrational states.

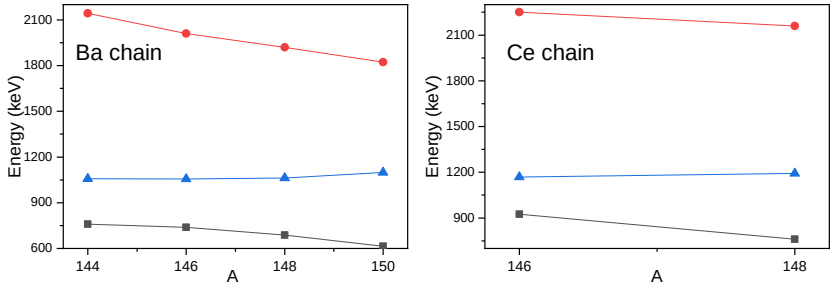

Fig. 4. Comparison of calculated and experimental energies of the lowest octupole vibrational states ($K = 0^-$ or 1^-). For notation, see Fig. 3.

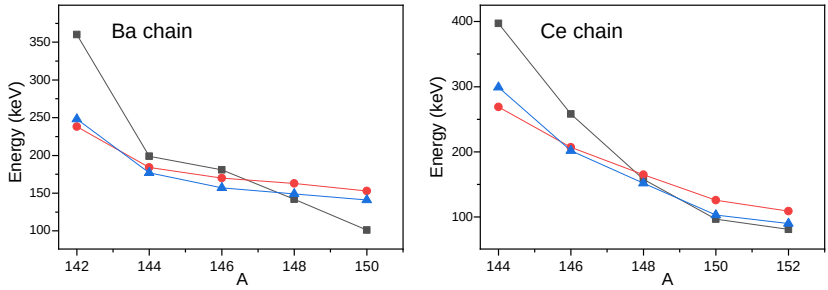

Fig. 5. Comparison of calculated and experimental energies of the lowest rotational state 2^+. For notation, see Fig. 3.

REFERENCES

[1] J.M. Allmond *et al.*, *Phys. Rev. Lett.* **118**, 092503 (2017).
[2] B. Moon *et al.*, *Phys. Rev. C* **95**, 044322 (2017).
[3] M. Jentschel *et al.*, *J. Instrum.* **12**, P11003 (2017).
[4] D.J. Rowe *et al.*, *Phys. Rev. C* **79**, 054304 (2009).
[5] M. Bender *et al.*, *Rev. Mod. Phys.* **75**, 121 (2003).
[6] H. Naidja *et al.*, *Phys. Rev. C* **96**, 034312 (2017).
[7] P.-G. Reinhard, *Ann. Phys. (Leipzig)* **504**, 632 (1992).
[8] A. Repko *et al.*, `arXiv:1809.01911 [nucl-th]`
[9] B. Pritychenko *et al.*, *Nucl. Data Sheets* **120**, 112 (2014).
[10] B. Bucher *et al.*, *Phys. Rev. Lett.* **116**, 112503 (2016).
[11] P. Klüpfel *et al.*, *Phys. Rev. C* **79**, 034310 (2009).
[12] W.J. Huang *et al.*, *Chin. Phys. C* **41**, 030002 (2017).
[13] J. Terasaki *et al.*, *Nucl. Phys. A* **600**, 371 (1996).
[14] J.A. Maruhn *et al.*, *Comput. Phys. Commun.* **185**, 2195 (2014).
[15] `http://www.nndc.bnl.gov/ensdf/`